T.3: First order magneto-structural phase transition in Fe-Rh based alloys and its implications on the functional properties

M. A. Manekar
Materials & Advanced Accelerator Sciences Division
E-mail: megh@rrcat.gov.in

1. Introduction

First order phase transitions are quite commonly experienced in our daily lives during phenomena like boiling of water into vapour or solidification of water into ice. These phase transitions have an associated latent heat of transformation [1]. Metastability and coexistence of the two competing phases involved in the transition are the other generic features of such first order transitions, irrespective of the underlying microscopic interaction or the nature of phases involved in the transition. It is more common to see the coexistence of water and ice over a broad temperature regime instead of a sudden transformation of the entire volume of water to ice. Such single shot transformations take place only in ultra-pure single element systems like Dy single crystals [2]. If we consider the water-ice system, it is observed experimentally that very pure water can be cooled well below 0^0 C (the thermodynamic transition temperature of water-ice system) without the formation of ice at normal atmospheric pressure. Water is then in a metastable state as it has a higher free energy than that of ice at the same temperature. Cooling below the thermodynamic transition temperature while still retaining the high temperature phase is termed as *supercooling* [3]. Similarly the low temperature phase can be *superheated* above the thermodynamic transition temperature before the transformation occurs. Thus the metastability across the phase transition leads to a hysteresis of the observed physical property as a function of the thermodynamic variable like temperature or pressure which drives the transition [3]. The observation of hysteresis can be a useful tool if the latent heat is difficult to measure across a first order phase transition [4]. The difficulty in measuring latent heat usually arises from the broadening of the phase transition due to underlying static quenched-in disorder in form of impurities, defects and dislocations in the system [5]. These impurities act as nucleation sites for the product phase in the parent matrix, e.g. dirt particles in water act as locations where the first nuclei of ice are formed. The impurity distribution thus influences the nucleation and growth dynamics which leads to interesting phenomenon as we see later during the course of this article. The influence of disorder on the kinetics of a first order transition can be so vital in certain cases that the survival of certain species solely depends on whether or not their body fluids freeze during the harsh winter conditions in the Arctic region. The Painted Turtle, for example, is known to keep its surface and internal organs so clean that it can prevent the solidification of body fluids down till temperatures as low as -15° C [6]. The survival of trees and certain fish near the North Pole without freezing are also some examples of tuning the nucleation and growth kinetics by controlling the levels of disorder.

First order transitions can also occur in form of a transformation from one lattice (or spin) structure to another within the solid state as a function of temperature, pressure and magnetic field [3, 4]. The same generic features of metastability and phase coexistence are observed across such transitions. While the nucleation and growth dynamics across a liquid-solid transition can influence the survival of certain species in nature, the same nucleation and growth dynamics across first order transitions in solids can be controlled in a laboratory to achieve a desired functional response of materials which can be of technological importance. One of the many ongoing activities at the Magnetic and Superconducting Materials Section (M&SMS) of RRCAT is related to this aspect of first order phase transitions [7]. Some of the functionalities that are being studied at the M&SMS are 1) ferromagnetic shape memory effect for actuator applications, 2) giant magnetoresistance for possible applications in data storage and 3) giant magnetocaloric effect to address the requirement of environmental-friendly refrigerator and regenerator materials for room temperature and cryogenic applications. In this article, we explore the characteristic features of a first order magneto-structural transition in a Fe-Rh based alloy system, which is known to have interesting functional properties of potential technological applications near room temperature. The work reported here has thus quite some relevance to the various research and development activities being carried out at RRCAT.

The Fe-Rh alloy system has attracted considerable interest due to giant magnetocaloric effect (MCE, change in temperature due to adiabatic application of magnetic field) [8], giant elastocaloric effect (change in temperature caused by mechanical stress) [9], giant magnetostriction (change in volume by the application of external magnetic field) [10] and giant magnetoresistance (GMR, change in electrical resistance by the application of external magnetic field) [11], occurring close to room temperature. We believe that such wide range of functionality of this alloy system arises due to a first order transition from an antiferromagnetic (AFM) to ferromagnetic (FM) state driven by both temperature (T) [12]

and magnetic field (H) [13]. This magnetic transition is also accompanied by a distortion in the crystal structure[13]. It was believed for quite some time that though Fe-Rh exhibits a giant MCE close to room temperature, the MCE vanishes after the first field cycle [14,15].

In this article we present the results of our work, which among other things has solved this long-standing problem. We show that the possible role of phase coexistence and associated metastability across the first order magneto-structural transition in tuning the functional properties of this material has largely gone unnoticed. Such phase coexistence and metastability across the first order magneto-structural transition (FOMST) in Fe-Rh alloys give rise to interesting thermomagnetic history effects in the observed physical properties like magnetization and magnetostriction. We clearly show that the vanishing of giant MCE in Fe-Rh was due to a lack of understanding of the thermomagnetic history effects, which are expected to occur across any first order transition driven by two variables like temperature and magnetic field. Apart from establishing the general nature of the thermomagnetic history effects, we also attempt to find the similarity between the nucleation and growth dynamics across a first order transition with the crystallization process of solids formed out of melts. This understanding is then used to model the response of a material exposed to multiple cycles of temperature inside the hysteretic region across a first order transition. We also show that under certain circumstances, the kinetics of the first order transition can get arrested and a glass-like state can arise which is now termed as the "magnetic glass". This article highlights that, apart from having a large value of the functional property (e.g. magnetocaloric effect or magnetostriction), it is also necessary to understand the nucleation and growth mechanism (which is governed by the underlying disorder) across a first order phase transition, if such materials are to be used for reproducible technological applications under multiple temperature or magnetic field cycles.

2. Experimental methods

The polycrsytalline parent Fe-Rh and Ni doped Fe-Rh alloys were prepared by arc melting the constituent elements in an argon atmosphere. Details of heat treatment and characterization can be found in ref. [16]. Temperature dependent ac susceptibility was measured using a home-made apparatus. Magnetization (M) measurements were performed using a commercial SQUID magnetometer (Quantum Design, MPMS-5) and Vibrating Sample Magnetometer (VSM, Quantum Design). Magnetic force microscopy (MFM) imaging was performed using a commercial instrument (NT-MDT, SOLVER-PRO). The linear thermal expansion was measured using a home-made set-up based on the strain gauge technique [17].

3. Phase coexistence: Bulk measurements

Phase coexistence across a FOMST has been widely studied in the case of manganites showing colossal magneto-resistance (CMR) [18,19]. Such phase coexistence is now observed in various other classes of magnetic materials like $CeFe_2$ based pseudobinaries [20] and giant magnetocaloric material namely Gd_5Ge_4 [21], suggesting the generality of this phenomenon. Such multi-scale phase coexistence which is observed even up to the micrometer scale can be explained by a coupling between the electronic and elastic degrees of freedom [22]. Here we first study the signatures of phase coexistence through bulk ac susceptibility measurements and then provide an explicit experimental evidence of the intricate relationship between structural and magnetic transition on the sub-micron scale in Fe-Rh using MFM.

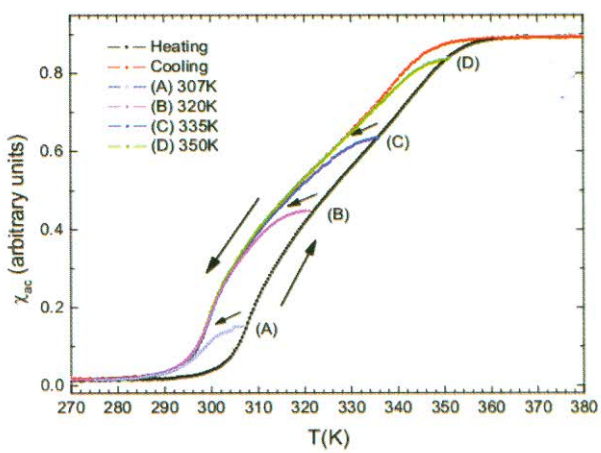

Fig. T.3.1: Temperature dependent ac susceptibility in a magnetic field of 3.4 × 10^{-4} T rms while heating and cooling the $Fe_{48}Rh_{52}$ sample.

Fig. T.3.1 shows ac susceptibility as a function of T across the AFM to FM transition both while heating and cooling the $Fe_{48}Rh_{52}$ sample. The transition has a thermal hysteresis of about 10K. The hysteresis curve which encloses both the reversible regions at the low-T and high-T end is known as the envelope curve. Phase coexistence across this transition can be verified by using the technique of minor hysteresis loops (MHL) [23]. A minor hysteresis loop is generated by reversing the direction of temperature change inside the hysteretic region on the envelope curve before reaching the reversible region. The minor loops showing hysteresis is an indication of the coexistence of the competing phases at the temperature of initiation of the loop. If there is no coexistence of the two phases, then the minor loops will not

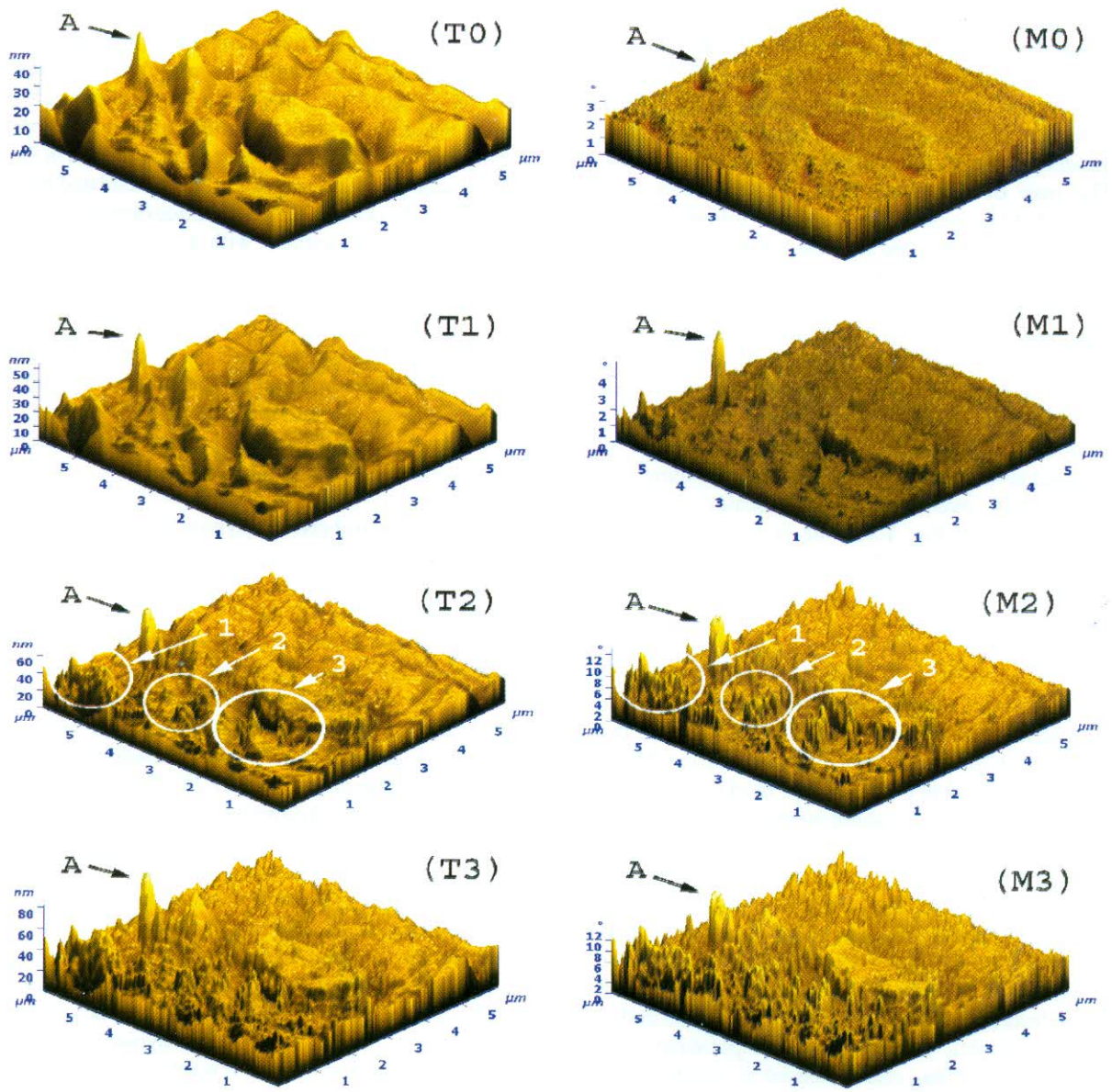

Fig. T.3.2: Time evolution of topography (T0, T1, T2 and T3) and the corresponding magnetic information (M0, M1, M2 and M3) obtained from Magnetic Force Microscopy measurements.

show any hysteresis. The other aspect to be noticed about the envelope curve is that the onset temperature of the AFM to FM transition during heating is nearly 300K while that of the FM to AFM transition while cooling is about 350K. A situation where the onset temperature while cooling is larger than that while heating, can arise mostly when the transition is influenced by disorder [24]. It is known that random quenched-in disorder can smear out a first order transition to an extent of complete rounding off of the transition [5]. Furthermore, strain produced in the sample matrix during a structural transition can couple these isolated defects and lead to the formation of a landscape of free-energy minima [22], which we discuss next.

4. Phase coexistence: Local measurements

The applicability of the landscape model can be verified by imaging the transition process using a local probe. Fig. T.3.2 shows the imaging of the time evolution of the AFM to FM transition in $Fe_{48}Rh_{52}$ using MFM. AC technique was used

for MFM imaging where the cantilever is oscillated at or near its resonance frequency. The magnetic interaction acts through a force gradient on the tip to produce a shift in the resonant frequency. This shift in the resonance frequency is detected in terms of shift in the phase of cantilever oscillation [25]. A non-zero phase shift indicates the presence of a FM cluster. The map of the phase shift over the scan area constructs the MFM image. The magnetic information is separated from the topographic information by performing the measurement in two different passes over the same region of the sample. The first pass provides the topography of the sample. This information is then used as a reference surface for the second pass with the tip lifted by about 30 nm. Thus the second pass measures forces originating mostly from magnetic interaction, which fall off much more slowly compared to the van der Waals forces [25]. Thus the MFM provides an unique tool for studying the lattice and magnetic part simultaneously over short length scales. For the measurements shown in Fig. T.3.2, the sample was dipped directly in liquid nitrogen (LN2) and then brought back to room temperature. With this temperature history, the sample is now mostly in the AFM state very close to the onset of the FM state as seen from Fig. T.3.1. This is also quite evident from the MFM image (M0) of Fig. T.3.2, where the FM state is yet to develop. To study the time evolution (dynamics) of the AFM to FM transition, we now focus our attention on the place marked as 'A' on the 3D topography and the MFM image of Fig. T.3.2. At time t=0, the place marked 'A' on the topography (T0) has a height of about 40 nm and is the largest defect site on the surface. This defect site acts as a nucleation centre for the first nucleus of the FM phase. The images (T1) and (M1) in Fig. T.3.2 were obtained after 1 hour. As can be seen, the magnetic signal (FM state) at location 'A' has increased to slightly more than 4^0 from a fraction of a degree in Fig. T.3.2 (M0). The AFM to FM transition is also coupled to a structural distortion in which the volume of the unit cell in the FM phase is slightly larger [13]. Correspondingly, the height of the location A has also increased to slightly more than 50 nm (see Fig. T.3.2 (T1)). After another 1 hour (t=2 h), new blisters appear on the topography (T2) and the MFM (M2) image. These regions are marked as 1, 2 and 3. At t=2h, the height of the location 'A' has also increased to almost 70 nm with a corresponding increase in the magnetic signal at the same location. Eventually after 3 hours, almost the entire sample surface gets crowded with these nuclei of the product FM phase ((T3) and (M3)). This observation shows that not only the growth of the individual nucleus but also the formation of newer nuclei is governed by the intricate coupling between the surface topography and the magnetic structure. These results show that a framework, which takes into account only static and isolated quenched-in disorder [5] to explain phase coexistence across the transition, could be quite insufficient. The formation of newer nuclei can be explained when a mechanism is present where the static impurities are correlated through a long-range field. In case where a system undergoes structural transition, cooperative lattice distortions and the associated modification in the strain fields provide a natural way to couple the isolated pockets of disorder already present [26]. The lattice distortion (change in topography) is accompanied with a coexistence of the two magnetic phases (Fig. T.3.2 (M2)). This observation follows the theoretical model, originally proposed for CMR manganites, by Ahn et al., [22] where the structural aspect is necessary to explain phase coexistence at micrometer scales. Our results on bulk and local measurements thus emphasize that phase coexistence and metastability are generic features associated with any system undergoing a FOMST and are not limited to only CMR manganites.

5. Nucleation and growth dynamics

Having established the phase coexistence through bulk and local measurements, we now try to find the common features between a general first order transition driven by temperature and magnetic field and the time dependent crystallization of solids from sufficiently supercooled melts. Crystallization process or the nucleation and growth dynamics, in general, during transformations in solids has been a subject of great interest [27.28]. The solidification and melting transitions are known to be of a first order nature and attempts have been carried out to establish the common features in such transitions with first order transitions in other systems. It has been shown that the vortex lattice in a type-II superconductor melts like ice melting to water [29]. To understand the common features of solidification process and other first order transitions, it is first necessary to measure the phase fraction of the competing phases and study its evolution with respect to the external thermodynamic variable like temperature or magnetic field. It is relatively straightforward to estimate the phase fraction using local imaging of the phase transition process [30], but quite difficult by using bulk measurements. The reason is that in a bulk measurement across a magnetic transition, the measured property like susceptibility or magnetization is a vector sum of all the individual values. We have studied the bulk magnetization and ac susceptibility across the first order AFM to FM transition in $Fe_{0.975}Ni_{0.025}Rh$ to establish the similarity of a general first order transition with that of a crystallization process [31]. The magnetic relaxation measurements across the temperature and field driven transition show a power-law dependence with a non-monotonic behaviour of the exponent as a function of temperature and magnetic field. This non-

monotonic behaviour of the exponent of this power law hints towards a nucleation and growth mechanism which is similar to the solidification process from melt [31]. The nucleation and growth mechanism of crystallization of solids from melt as a function of time is described phenomenologically by the Avrami model [32]. The central assumptions of the Avrami model are as follows:

- The new phase is nucleated by germ nuclei which already exist in the parent matrix.
- The density of these germ nuclei diminishes through activation of some of these into growth nuclei and the coalescence of these nuclei in to the product phase.
- The growth rate is independent of the transformed phase and only depends on the untransformed phase
- The nucleation events are considered to be random and the nuclei are allowed to freely overlap with each other during the growth process.

This model gives the evolution of phase fraction as a function of time in terms of an equation:

$$f = 1 - \exp(-kt^{\eta}) \quad (1)$$

and is known as the Kolmogorov-Johnson-Mehl-Avrami (KJMA) relation. Here 'k' is related to the activation energy and 'η' is the Avrami exponent, which is related to geometrical factors. This equation gives the famous 'S' shaped curve when the phase fraction is plotted as a function of time. As mentioned earlier, the relaxation measurements of bulk magnetization show a time dependence which is a power law and not the same as predicted by the KJMA relation. We have therefore proposed that the area of MHLs can be treated as the measure of phase fraction during the phase transition. The generalization of the Avrami law from 'time' to 'temperature' or 'field' can then be carried out by studying the evolution of phase fraction across the corresponding phase transitions. Fig. T.3.3 shows the normalized area of MHLs with respect to the area under the envelope curve (or the phase fraction). The curve resembles the 'S' shaped curve and can be fitted by the relation:

$$f = 1 - \exp(-k(T-T_0)^{\eta}) \quad (2)$$

Here T_0 is the onset temperature of the transition. The same relation holds true even for field induced transition with 'T' replaced by 'H'.

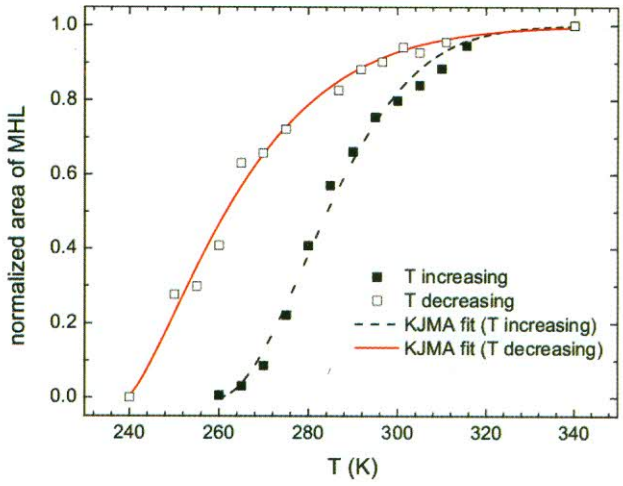

Fig. T.3.3: Temperature dependence of the areas of MHLs inferred from the ac susceptibility measurements on $Fe_{0.975}Ni_{0.025}Rh$. The areas of MHLs are related to the phase fraction of the ferromagnetic phase.

Fig. T.3.4 shows the evolution of phase fraction as a function of magnetic field and the fit of the experimental data with the KJMA curve. The phase fraction across the field-induced transition can be fitted with

$$f = 1 - \exp(-k(H-H_0)^{\eta}) \quad (3)$$

where H_0 is the onset field of transition. These results show that the area of MHLs can be indeed treated as a

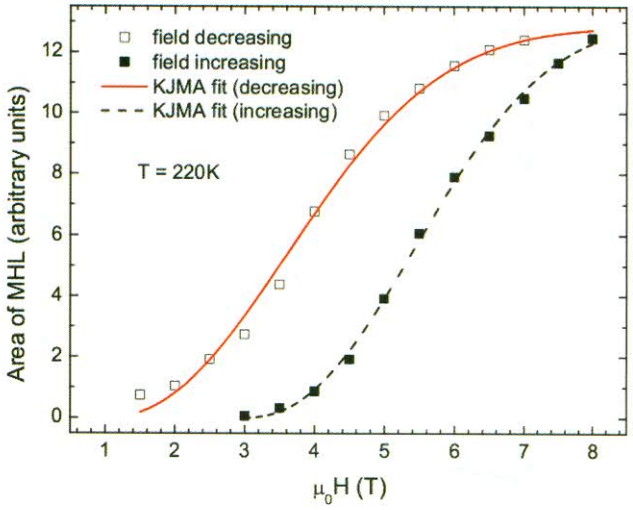

Fig. T.3.4: Magnetic field dependence of the areas of MHLs during magnetization measurements on $Fe_{0.975}Ni_{0.025}Rh$.

measure of the phase fraction of the competing phases across the phase transition. The heuristic argument for taking the area of MHL as the phase fraction is as follows. The envelope curve is the hysteresis curve which encloses both the reversible low-temperature and high-temperature phases. During the heating cycle of the envelope curve, the entire sample transforms from the AFM to FM phase. Similarly, the cooling curve represents the entire sample transforming from the FM to AFM phase. If a minor loop is initiated at any intermediate temperature value, it exhibits a smaller hysteresis compared to the hysteresis obtained on the complete envelope curve. A minor loop shows hysteresis when both the phases involved in the transition coexist. The MHL initiated at a lower temperature encloses a smaller area compared to MHL initiated at a higher temperature as the amount of the FM phase at lower temperatures is lower during the heating cycle. Thus growing FM fraction is also accompanied with the growing area of MHL. If we (hypothetically) divide the entire sample into smaller volumes, each hysteresis loop (envelope curve or MHL) can be thought of as a superimposition of smaller hysteresis loops for each of these volumes. Thus the area of a hysteresis loop initiated at any temperature, which is an addition of smaller hysteresis loops, would represent the volume of the transformed phase at that temperature. If we take the area of envelope curve as unity, the normalized area of each MHL can then be taken as the phase fraction of the product phase at the temperature of initiation of MHL.

6. Modeling of minor hysteresis loops

The assumption of different locations of the sample having their own independent hysteresis was explored further by measuring thermal expansion across the transition in $Fe_{0.955}Ni_{0.045}Rh$ [33]. Fig. T.3.5 shows some of the representative MHLs in strain measurements,

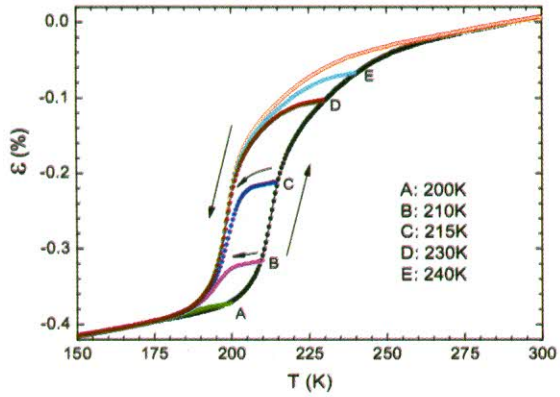

Fig. T.3.5: Strain v/s Temperature during heating and cooling in $Fe_{0.955}Ni_{0.045}Rh$ and representative minor hysteresis loops on the heating cycle.

which are initiated during the heating cycle across the first order transition in $Fe_{0.955}Ni_{0.045}Rh$. The presence of hysteresis and phase coexistence (resulting in MHLs) across the transition means that the value of the measured physical property not only depends on the value of the driving force (temperature, in this case) but also on the history of reaching to a particular value of the control parameter. The output is then a multivalued function of the input. This fact is of significant importance if the physical property (presently, strain) is to be used for technological applications where the device undergoes numerous cycling of the driving force. Specifically, if the material is cycled to and fro inside the hysteretic regime, it becomes necessary to be able to predict the entire path of evolution of the output if a successful device is to be constructed.

The MHLs inside the hysteretic region were modeled using the Preisach model of hysteresis which was originally proposed for explaining the hysteresis of ferromagnets [34]. The basic assumption of the Preisach model is that the complete hysteresis curve can be thought of as a summation of elementary hysteresis operators (or hysterons) defined in Fig. T.3.6. This assumption is similar to the one used for identifying the phase fraction discussed earlier. The switching operator is chosen such that $\gamma_{\alpha\beta} \times T$ is either 0 or 1, where T is the input. The value of the hysteresis operator switches to 1 at $T = \alpha$ on the T-increasing cycle and switches back to 0 at $T = \beta$ during the T-decreasing cycle. The output $\varepsilon(T)$ is then given by,

$$\varepsilon(T) = \iint_{\alpha \geq \beta} \mu(\alpha, \beta)[\gamma_{\alpha\beta} T]\, d\alpha\, d\beta \qquad (4)$$

where $\mu(\alpha\beta)$ is the weight factor associated with each hysteresis operator.

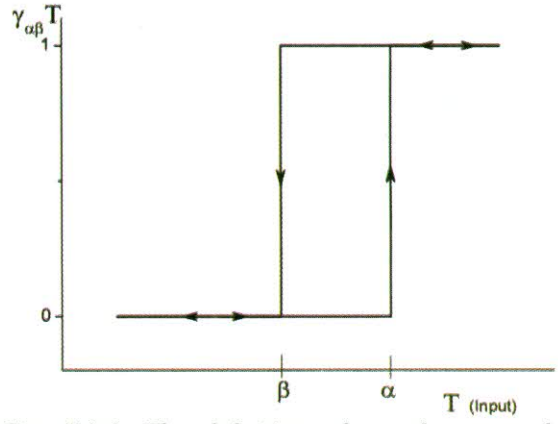

Fig. T.3.6: The definition of an elementary hysteresis operator according to the Preisach model.

By using this relation, the behaviour of MHLs can be modeled for multiple temperature cycles. More details of this calculation can be found in ref. [33] which uses the experimental data at close temperature steps.

Fig. T.3.7 shows one such case of two MHLs generated for multiple temperature cycles. The bigger MHL is generated by decreasing the temperature from α_1 to β_1, subsequently increasing the temperature to α_2 and then finally reducing the temperature to below β_1. The innermost MHL is generated by following the path α_1-β_1-α_2-β_2-α_3 and then reducing the temperature to β_3. The solid lines are the calculated curves using equation 4 which describe the experimental results quite well. However, the Preisach model fails beyond a certain temperature or at the 'tails' of the transition, where there is a crossover from nucleation dominated process to growth oriented process. More details can be found in ref. [33]

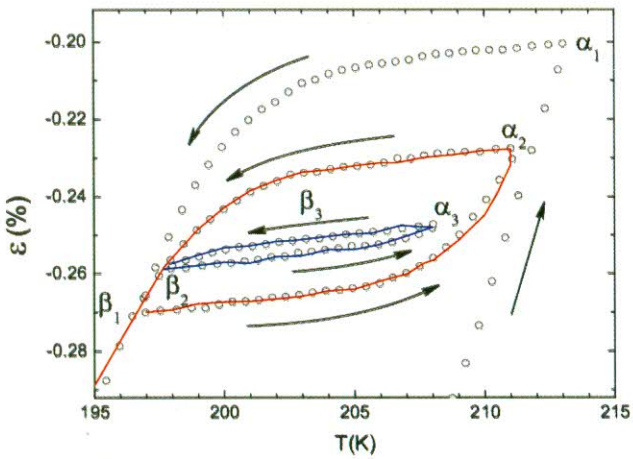

Fig. T.3.7: The experimental data (open circles) along with the calculated curves using the Preisach model as described in Eq. (4)

7. Thermomagnetic history effects

So far we have discussed the history effects arising due to the nucleation and growth process across a first order transition driven by only a single variable like temperature. Interesting history effects also arise when the transition is driven by two thermodynamic variables like temperature and magnetic field. We show that the study of such phase coexistence and related history effects is important because they influence the functional properties of Fe-Rh like the giant MCE near room temperature [35]. We also show how the understanding of these history effects can be used to achieve reproducible response from a material which undergoes a first order transition.

Fig. T.3.8 shows isothermal M-H curves across the field induced transition in the parent Fe-Rh alloy at two representative temperatures, which are 290K and 305K. For both the measurements, the sample was warmed up to these temperatures in zero field from temperatures well below 200 K, where the sample is completely in the AFM state [16].

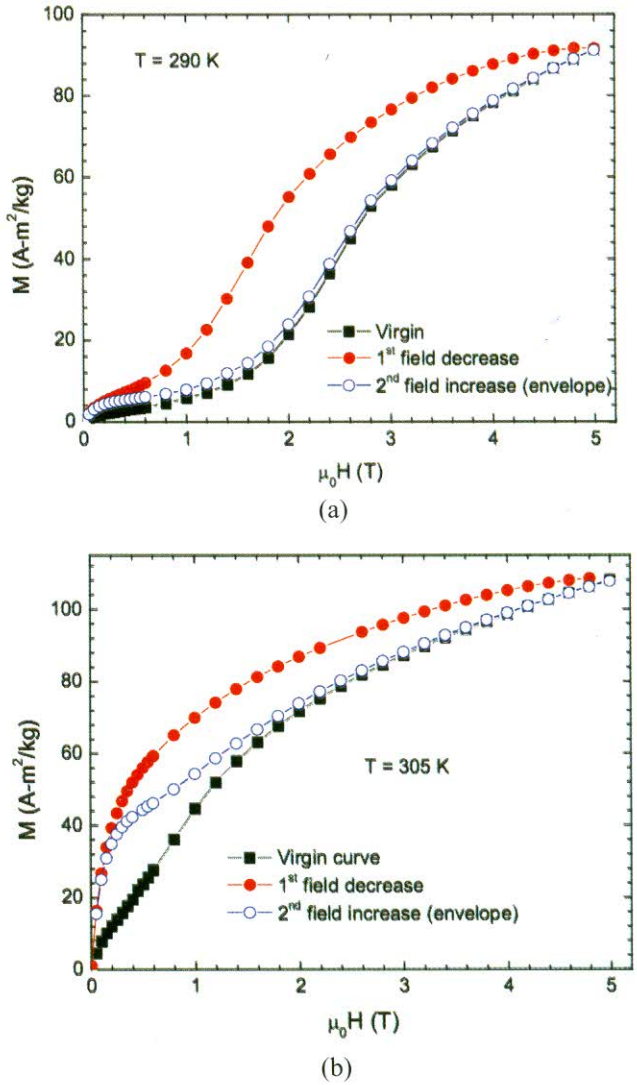

Fig. T.3.8: Isothermal magnetization as a function of field at (a) 290K and (b) 305 K

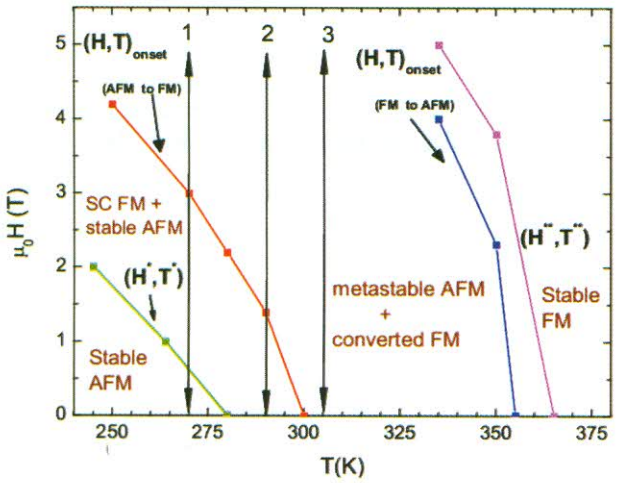

Fig. T.3.9: H-T phase diagram of $Fe_{48}Rh_{52}$

A sudden increase in magnetization during the first field increase (virgin curve) is a signature of a field induced (metamagnetic) transition. The transition shows a hysteretic behaviour on decreasing the field. The nature of the hysteresis across the transition is quite different compared to the M-H hysteresis observed in case of ferromagnets. On the second H-increasing cycle (envelope curve) we see that the virgin curve lies outside the envelope curve. During subsequent isothermal H cycles, the envelope curve is retraced irrespective of the number of cycles and the virgin curve is lost for that isothermal M-H cycle.

The phenomenon of the virgin curve lying outside the envelope curve can be explained by using the H-T phase diagram for our Fe-Rh alloy, which is shown in Fig. T.3.9. This H-T phase diagram has been determined through a detailed study of ac susceptibility and magnetization [16]. The (H*, T*) line marks the limit of supercooling of the FM phase. Between the (H*, T*) line and the $(H, T)_{onset}$ (AFM to FM) line, the supercooled FM phase (SC FM) can coexist with stable AFM phase during the T and/or H decreasing cycle. Beyond the (H**, T**) line, the sample is in the stable FM phase. In the region between the $(H, T)_{onset}$ (AFM to FM) and (H**, T**) lines, the sample is in the phase coexistent state where the partly converted FM phase coexists with the metastable AFM phase. The fraction of the AFM phase decreases as the (H**, T**) line is approached by either increasing T or H [16]. For the isothermal H-increasing cycle at 290K shown in fig. T.3.8(a) (the path marked as 2 in Fig. T.3.9), the starting point of the isothermal H cycle is single phase stable AFM. The sample partly gets converted to FM phase during the isothermal increase in H. This FM phase can be supercooled when H is isothermally reduced back to zero and then leads to a higher value of M on the subsequent H-increasing cycles. For the isothermal H-increasing cycle at 305K shown in Fig. T.3.8(b) (the path marked as 3 in Fig. T.3.9), the starting condition of the sample is that of a small fraction of partly converted FM phase coexisting with a large fraction of the AFM phase. Most of this AFM phase gets converted to stable FM phase during the isothermal increase in H. This FM phase persists even when H is isothermally reduced back to zero [16] and is then carried over during the next isothermal H-increasing cycle giving rise to higher value of M on the envelope curve. This observation shows that if the working temperature of Fe-Rh is to be confined between 280 and 360 K, which could be of interest for magnetic refrigeration near room temperature, the virgin curve will always be outside the envelope curve. This loss of virgin curve was thought to be the cause behind the vanishing of MCE after the first field cycle [8, 14, 15].

8. Influence of history effects on functional property

With this background, we proceed to estimate the change in magnetic entropy (magnetocaloric effect) for an isothermal cycle. The magnetic entropy is calculated by using the integral Maxwell relation approximated for M-H curves measured at discrete T intervals [36] and is given by,

$$\Delta S_m \approx \frac{1}{\Delta T}\left[\int_0^H M(T+\Delta T,H)dH - \int_0^H M(T,H)dH\right] \qquad (5)$$

Thus the area under the isothermal M-H curve from 0 to upper limit H (5 T in our case) at a particular temperature T can be subtracted from the area under the M-H curve at a higher temperature $T + \Delta T$ to estimate the change in magnetic entropy at the temperature $(T + \Delta T/2)$. Each isothermal measurement during the H-increasing cycle gives the virgin curve and the envelope curve. This gives four combinations for calculating the ΔS_m,. These are:

(1) area under the virgin M-H curve at T to be subtracted from area under the virgin M-H curve at $T + \Delta T$,

(2) area under the virgin M-H curve at T to be subtracted from area under the envelope M-H curve at $T + \Delta T$,

(3) area under the envelope M-H curve at T to be subtracted from area under the virgin M-H curve at $T + \Delta T$, and

(4) area under the envelope M-H curve at T to be subtracted from area under the envelope M-H curve at $T + \Delta T$.

The MCE in Fe-Rh is inverse, i.e. the sample cools by adiabatic increase in H [8]. If the adiabatic H-increasing cycle

is started at the zero-field point of path 3 in Fig. T.3.9, the sample reaches at the $\mu_0 H = 5$ T point at a lower T (say path 2). When H is reduced isothermally along path 2, some amount of FM phase will remain supercooled as discussed earlier. This means that even if the adiabatic cycle is started in the virgin

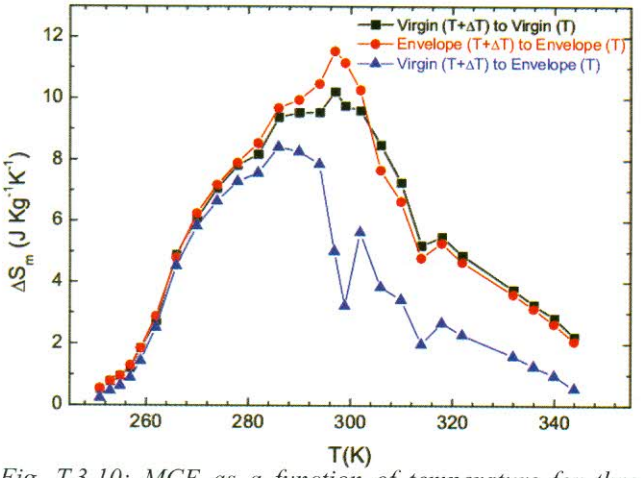

Fig. T.3.10: MCE as a function of temperature for three possible histories of the sample.

state at a higher temperature, the low temperature state corresponds to the envelope curve. Thus the second mathematical possibility of subtracting the area under the virgin M-H curve at T from the area under the envelope curve at T + ΔT cannot be achieved physically and has to be ruled out. Also, the first possibility from the above list would be difficult to achieve physically but we still retain it for the sake of comparison.

Fig. T.3.10 shows the ΔS_m as a function of T for the three possible histories listed above [37]. The variation in MCE clearly shows the history dependence. It can be clearly seen that when the difference between the areas of the virgin curve at a higher temperature and the envelope curve at a lower temperature is taken, the MCE reduces drastically compared with the differences in areas of the virgin curves at the same temperatures. This is what was noted by Annaorazov *et al* [8] and has later been accepted generally. We, however, see that if the difference in areas between two envelope curves is taken, the MCE actually increases marginally compared with the virgin cycle. Thus for a refrigeration cycle using Fe-Rh, the first H-increasing and decreasing cycle at higher temperature needs to be isothermal. The adiabatic H-increasing cycle can then be carried out during the second field increase to achieve a high entropy change. If the envelope curve is used for magnetic cooling, the effective refrigerant capacity R_{eff} (i.e. refrigerant capacity after subtracting the hysteresis loss) turns out to be 324.42 J kg^{-1} with the hot end at 311.8 K and cold end at 268.6K of the refrigerator.

We have used this method of achieving a reproducible MCE across the first order AFM to FM transition in $Fe_{0.975}Ni_{0.025}Rh$. A very large effective refrigerant capacity of 492.8 J kg^{-1} with the hot end of the refrigerator at 307.1K and the cold end at 230.5K has been achieved [38]. This is probably the highest known R_{eff} for any material world-wide at room temperature.

9. Glassy dynamics across first order transition

So far we have seen the influence of disorder on the first order phase transition and how the functional properties, especially their repeatability, depend on the history effects that arise as a result of disorder. The disorder can be used to tune the transition parameters like the onset temperatures and the width of the transition to achieve the desired functionality. However, increasing the disorder may not always tune the desired properties in a monotonic manner but can lead to an entirely new phenomenon.

We now present the results of magnetization relaxation measurements and thermomagnetic history effects across the FM to AFM transition in $Fe_{0.955}Ni_{0.045}Rh$. The higher concentration of Ni appears to have an effect of arresting the kinetics of the first order FM to AFM phase transition. This kinetic arrest of the first order phase transition gives rise to a glass-like nonequilibrium state [39]. Fig. T.3.11 shows magnetization as a function of temperature in an applied field of 10 mT under different thermomagnetic histories.

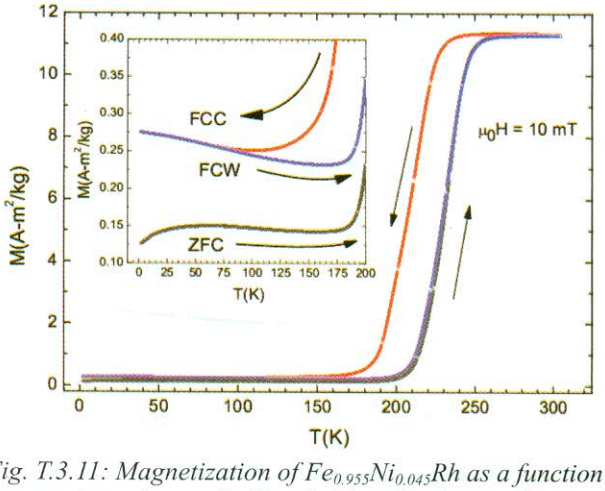

Fig. T.3.11: Magnetization of $Fe_{0.955}Ni_{0.045}Rh$ as a function of temperature in a field of 10 mT. Inset shows the thermomagnetic irreversibility on an expanded scale at lower temperatures.

In the zero-field-cooled (ZFC) protocol, the sample is cooled from above 300 K to the lowest temperature in zero field. The field is then switched on and magnetization is measured during warming up the sample. After reaching above 300 K, the magnetization is measured while cooling the sample unidirectionally without switching off the field. This measurement protocol is known as field-cooled-cooling (FCC). Once the lowest temperature is reached during the FCC, the sample is warmed up again in the same constant applied field. The resulting M-T curve is denoted as the field-cooled-warming (FCW) curve. The rise in magnetization at around 180 K (see inset of Fig. T.3.11) in the ZFC curve, marks the onset of the transition from the AFM to the FM phase. On cooling from above 300 K there is a marked hysteresis across the transition, which is typical of a first order transition. On further cooling down to the lowest temperature, we observe that the transition is not complete and the FCC magnetization curve does not merge with the ZFC magnetization curve (see inset of Fig. T.3.11). The FCC magnetization curve would have merged with the ZFC magnetization curve in the event of completion of the FM to AFM transition. This thermomagnetic irreversibility (TMI) gives the first indication that the kinetics of the FM to AFM transition are arrested [40,41]. However, such TMI between the ZFC and FCC magnetization curves can also arise in case of a spin glass [42] and in case of systems with long range ferromagnetic order [43]. However, the possibility of a spin glass transition or ferromagnetic impurity is ruled out in the present system as the TMI further increases with increase in applied field [39] (results not shown here for the sake of conciseness). This nature of TMI is clearly opposite to the trend observed in case of spin glass [44] and ferromagnets [43] It has been shown that such thermomagnetic history effects are the outcome of the kinetics of the first order transition getting arrested by the application of magnetic field [44], resulting in a magnetic-glass.

We now focus on the kinetics of the ferromagnetic to antiferromagnetic transition in the $Fe_{0.955}Ni_{0.045}Rh$ alloy during the FCC protocol in a field of 5T, by observing the time dependent magnetization at certain temperatures. At higher temperatures, i.e. near the FM to AFM transition while cooling, the relaxation can be described by the following power law [39]:

$$M(T)/M_0 = -1 + 2t^{\gamma} \qquad (6)$$

However, at lower temperatures, when the AFM phase has formed in sufficient quantities, the relaxation cannot be explained in terms of a single simple equation. The relaxation is described with a combination of the following laws [39]:

$$A_1(T)(-1 + 2t^{\gamma}) + A_2(T)(\exp[(-t/\tau)^{\beta}]) \qquad (7)$$

The second term is the stretched exponential function with β which ranges between 0.6 to 0.9 and τ is the time constant. $A_1(T)$ and $A_2(T)$ are the temperature dependent weight factors for the power law and stretched exponential parts of equation. The stretched exponential function is a characteristic of glassy dynamics [45] and has been used earlier for explaining the time dependence of magnetization observed during the formation of magnetic-glass in various systems like doped $CeFe_2$ alloys [40],

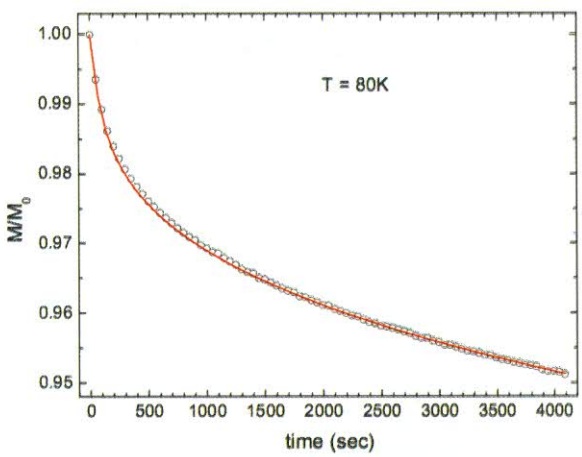

Fig. T.3.12: Time dependence of magnetization of $Fe_{0.955}Ni_{0.045}Rh$ during the FCC protocol in 5T field at one representative temperature. The solid line is a fit to equation 7.

NiMnIn based off-stoichiometric Heusler alloys [46] and Gd_5Ge_4 [47]. The power law represents the relaxation in the crystalline phase [39].

Fig. T 3.12 shows a relaxation measurements at one representative temperature. The time dependence of magnetization can be fitted with Eq. (7). The relative weights, $A_1(T)$ and $A_2(T)$ are found at various temperatures to see how the transformation proceeds with temperature.

A plot of A_1 and A_2 as a function of temperature in Fig. T.3.13 gives a qualitative picture of how the crystalline and glassy phases evolve with temperature out of the unconverted FM phase. It can be seen that the glassy dynamics appear just below 110 K, after a substantial amount of FM phase has already been converted to the equilibrium AFM state.

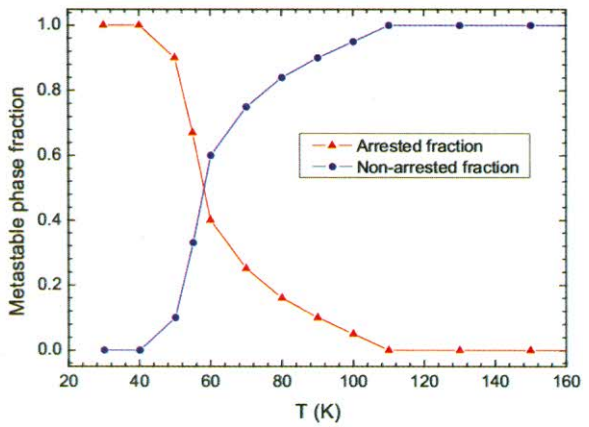

Fig. T.3.13: Relative phase fractions of the non-arrested and arrested phases across the FM to AFM transition in $Fe_{0.955}Ni_{0.045}Rh$ during the FCC protocol at 5T.

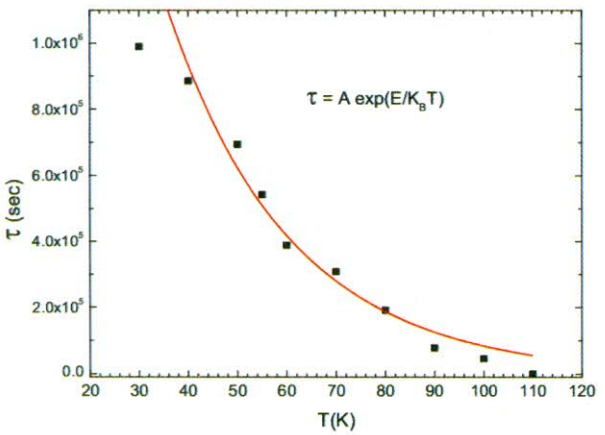

Fig. T.3.14: The temperature dependence of the time constant in the stretched exponential term of equation 7. Solid squares are the experimental data. The solid line is a fit to the data using equation 8.

It can be inferred that the growth of the product phase (AFM in this case) itself influences the arrest of the kinetics of the FM to AFM transition [39]. The glassy phase thus seems to be an outcome of the disorder influenced nucleation and growth dynamics across the first order transition.

Liquids which undergo glassy transitions are categorized as strong or fragile depending on the how the viscosity or the time constant of the stretched exponential varies with temperature [45] With analogy to this framework, in our case the liquid state corresponds to the ferromagnetic phase. The temperature dependence of follows the Arhenius function given by:

$$\tau = A\exp(E / K_B T) \quad (8)$$

where E is the activation energy and K_B is the Boltzmann constant. Fig. T.3.14 shows the temperature dependence of in the stretched exponential term of Eq. (7) along with the fit to Eq. (8). The Arhenius functionality of the time constant indicates that the ferromagnetic phase behaves as a strong glass forming liquid.

Conclusion

In conclusion, we have studied the nucleation and growth dynamics across the disorder influenced first order magneto-structural transition in Fe-Rh based alloy system. The thermomagnetic history effects arising due to phase coexistence across this transition are shown to influence the response of the material for multiple temperature and magnetic field cycles. Contrary to the long held belief, a reproducible magneto-caloric effect with a large refrigerant capacity at room temperature could be achieved by understanding these history effects. The disorder is not only important in tuning the functionality in alloys, but also can lead to an entirely new phenomenon like the kinetic arrest of the phase transition.

Acknowledgements

This work was done as a part of my Ph.D. thesis work. I am thankful to my thesis advisor Dr. S. B. Roy for his guidance and other members of M&SMS for their support.

References

1) Reichl L. E., A modern course in statistical physics (John Wiley & Sons, Inc., New York, 1998), 2nd ed.
2) Pecharsky V. K., et al., Scr. Mater. 35, 843 (1996)
3) Chaikin P. M. and Lubensky T. C., Principles of condensed matter physics (Cambridge University Press, Cambridge, 1995).
4) White R. M. and Geballe T. H., Long range order in solids (Academic Press, New York, 1979).
5) Imry Y. and Wortis M., Phys. Rev. B 19, 3580 (1979)
6) Packard G. C. et al., J. Exp. Biol, 204, 1667 (2001)
7) Roy S. B. J. Phys.: Condens. Matter, 25, 183201 (2013).
8) Annaorazov M. P. et al., J. Appl. Phys., 79, 1689 (1996).

9) Nikitin S. A. et al., Phys. Lett. A, 171, 234 (1992).
10) Ibarra M. R. and Algarabel P. A., Phys. Rev. B 50, 4196 (1994).
11) Algarabel P. A. et al., Appl. Phys. Lett. 66, 3061 (1995)
12) Kouvel J. S. et al., J. Appl. Phys. 33, 1343 (1962).
13) Zakharov A. I. et al., Sov. Phys. JETP, 19, 1348 (1964).
14) Pecharsky V.K. and Gschneidner K.A., Jr., J. Mag. Mag. Mater. 200, 44 (1999).
15) Pecharsky V.K. and Gschneidner K.A., Jr., Phys. Rev. Lett., 78, 4494 (1997).
16) Manekar M. and Roy S. B., Eur. Phys. J. B. 64,19 (2008)
17) Sharma V. K., Ph.D. thesis, Homi Bhaha National Institute, Raja Rammana Centre for Advanced Technology, Indore (2012),
18) Dagotto E., Nanoscale Phase Separation and Colossal Magnetoresistance: The Physics of Manganites and Related Compounds (Springer, Berlin) 2003.
19) Dagotto E, New J. Phys. 7, 67 (2005).
20) Roy S. B. et al., Phys. Rev. Lett. 92, 147203 (2004)
21) Moore J. D. et al., Phys. Rev. B 73 144426 (2006)
22) Ahn K. H. et al., Nature, 428, 401 (2004).
23) Manekar M. et al., J. Phys.: Condens. Matter 12, L409 (2000).
24) Chattopadhyay M.K. et al., Phys. Rev. B 68, 174404 (2003)
25) Zhu Y ed. Modern Techniques for Characterizing Magnetic Materials (Kluwer Academic, USA) 2005
26) Burgy J et al., Phys. Rev. Lett., 92, 097202 (2004).
27) Christian J. W., The theory of transformations in metals and alloys (Pergoman Press, Amsterdam, 2002), 3rd ed.
28) Porter D. A. and Easterling K. E., Phase transformation in metals and alloys (Chapman & Hall, London, 1992)
29) Zeldov E. et al., Nature 375, 373 (1995).
30) Soibel A. et al., Nature 406 282 (2000).
31) Manekar M. and Roy S. B. J. Phys.: Condens. Matter 20, 325208 (2008).
32) Avrami M., J. Chem. Phys 7, 1103 (1939).
33) Manekar M., et al., J. Phys.: Condens. Matter, 24, 216004 (2012).
34) Mayergoyz I, Mathematical models of hysteresis and their applications (Elsevier Science, NY 2003), 2nd ed.
35) Manekar M and Roy S. B., J. Phys. D: Appl. Phys. 41, 192004 (2008)
36) McMichael R. D. et al., J. Appl. Phys. 73, 6946 (1993).
37) Manekar M. and Roy S. B., J. Phys. D: Appl. Phys. 41 192004 (2008)
38) Manekar M. and Roy S. B., J. Phys. D: Appl. Phys. 44, 242001 (2011).
39) Manekar M., et al., J. Phys.: Condens. Matter 23, 086001 (2011).
40) Chattopadhyay M. K., et al., Phys. Rev. B. 72,180401(R) (2005)
41) Manekar M, et al., Phys. Rev. B. 64, 104416 (2001).
42) Mydosh J. A., Spin Glasses (Taylor & Francis, London, 1992).
43) Roy S. B., et al., Solid State Commun. 99, 563 (1996)
44) Roy S. B. and Chattopadhyay M. K., Phys. Rev. B. 79, 052407 (2009)
45) Debenedetti P. G. and Stillinger F. H., Nature 410, 259 (2001).
46) Sharma V. K. et al., Phys. Rev. B. 76, 140401(R) (2007)
47) Roy S. B., et al., Phys. Rev. B. 74, 012403 (2006)